Investigation of Magnetic Ordering in $RCo_{12}B_6$ (R = Y, Nd) by ^{57}Fe Mössbauer Spectroscopy*

J. M. Cadogan,[A] *S. J. Campbell,*[B] *X. L. Zhao*[B,C] *and E. Wu*[B]

[A] School of Physics, University of New South Wales,
Kensington, N.S.W. 2033, Australia.
[B] Department of Physics, University College, University of New South Wales,
Australian Defence Force Academy, Canberra, A.C.T. 2600, Australia.
[C] On leave from Applied Acoustics Institute, Shaanxi Teachers University,
Xian, P.R. China.

Abstract

Mössbauer spectra of $YCo_{12}B_6$ and $NdCo_{12}B_6$ doped with enriched ^{57}Fe have been obtained at various temperatures between $4 \cdot 2$ K and room temperature. The spectrum of $YCo_{12}B_6$ at $4 \cdot 2$ K indicates that the Co sublattice orders in the crystallographic basal plane. $NdCo_{12}B_6$ orders along or close to the crystallographic c-axis at $4 \cdot 2$ K and undergoes a spin-reorientation with increasing temperature until at ~ 55 K the magnetisation lies in or near the basal plane.

1. Introduction

The magnetic properties of the ternary rare-earth (R) intermetallics with the composition $RCo_{12}B_6$ have been studied by a number of groups (e.g. Jurczyk *et al.* 1987; Rosenberg *et al.* 1988; Mittag *et al.* 1989; Rosenberg *et al.* 1992; Campbell *et al.* 1993). These compounds crystallise in the rhombohedral $SrNi_{12}B_6$ structure (Niihara and Yajima 1972; Chaban and Kuz'ma 1977; Stadelmaier and Lee 1978; Kuz'ma *et al.* 1981) with the space group $R\bar{3}m$. The R atoms occupy the $3a$ crystallographic sites, the Co atoms occupy the $18g$ and $18h$ crystallographic sites, and the B atoms occupy $18h$ crystallographic sites, in the standard Wyckoff notation.

Rosenberg *et al.* (1992) carried out a thorough investigation of the magnetic properties and ^{57}Fe Mössbauer spectroscopy of rare-earth compounds of the type $RFe_{12-x}Co_xB_6$ ($x \le 10$ for R = La; $x = 11 \cdot 8$ for R = Y and Gd). An aim was to understand the unusual behaviour of the ferromagnetic ordering temperature exhibited by the 1-12-6 type of system compared with other systems in which cobalt is substituted for iron. For example, ferromagnetic ordering appears to vanish around $s \sim 0 \cdot 25$ in the $Nd(Fe_{1-s}Co_s)_{12}B_6$ system, reappearing at higher cobalt concentration $s \sim 0 \cdot 35$ (Buschow 1987). In the case of the $LaFe_{12-x}Co_xB_6$ system, Rosenberg *et al.* (1992) linked the behaviour of the ferromagnetic ordering temperature with the unstable character of the iron moment. They further linked the partial collapse of the 3d sublattice moment at intermediate concentrations with preferential site occupation for the cobalt and iron atoms. In common with

---

* Paper presented at the Festschrift Symposium for Dr Geoffrey Fletcher, Monash University, 11 December 1992.

the results obtained by Rosenberg *et al.* (1992) for $LaFe_{12-x}Co_xB_6$ ($x \leq 10$), $YFe_{0\cdot2}Co_{11\cdot8}B_6$, $GdFe_{0\cdot2}Co_{11\cdot8}B_6$, Campbell *et al.* (1993), in a ^{57}Fe Mössbauer study of $NdCo_{12}B_6$ doped with enriched ^{57}Fe, demonstrated that the Fe atoms exhibit a strong preference for occupying the 18*h* site rather than the 18*g* site. This earlier study (Campbell *et al.* 1993) serves as a precursor to the present study, the main purpose of which is to investigate the magnetic structures of $YCo_{12}B_6$ and $NdCo_{12}B_6$ by ^{57}Fe Mössbauer-effect spectroscopy. The impetus for this study was the observation of an anomaly in the temperature dependence of the magnetisation of $NdCo_{12}B_6$ observed by Mittag *et al.* (1989), although quite different behaviour was observed by Jurczyk *et al.* (1987). Our aim was to search for a possible spin-reorientation in $NdCo_{12}B_6$ which may be responsible for this anomaly.

2. Experimental

The samples of $YCo_{12}B_6(^{57}Fe)$ and $NdCo_{12}B_6(^{57}Fe)$ used in this study were prepared from high-purity metals ($99\cdot99\%$ Y and Nd, $99\cdot998\%$ Co and $99\cdot5\%$ B) by standard arc melting in an atmosphere of purified argon. The extent of the doping with $97\cdot5\%$ enriched ^{57}Fe amounted to $0\cdot5$ wt%. The arc-melted samples were wrapped in Ta foil and annealed in sealed evacuated quartz tubes at 900°C for three weeks.

Powder X-ray diffraction (XRD) with Cu Kα radiation was used to characterise the samples. The diffraction patterns of both samples exhibited all the peaks of the rhombohedral $SrNi_{12}B_6$ structure (Niihara and Yajima 1972; Chaban and Kuz'ma 1977; Stadelmaier and Lee 1978; Kuz'ma *et al.* 1981). The lattice parameters of our samples were $a = 9\cdot491$ Å and $c = 7\cdot458$ Å for $NdCo_{12}B_6(^{57}Fe)$, and $a = 9\cdot463$ Å and $c = 7\cdot462$ Å for $YCo_{12}B_6(^{57}Fe)$. The XRD pattern of $NdCo_{12}B_6(^{57}Fe)$ shows the presence of Co_2B- and Co-type impurity phases, while the $YCo_{12}B_6(^{57}Fe)$ pattern shows Co_2B and Y_2O_3 impurities. The extent of the impurity phases will be mentioned later in the light of the Mössbauer results. Further details on the samples and their preparation are presented elsewhere (Campbell *et al.* 1993).

Mössbauer spectra were obtained at various temperatures between $4\cdot2$ K and room temperature (20±1°C) using a standard transmission spectrometer (Jing *et al.* 1992). A ^{57}CoRh source was used in the Mössbauer experiments and the spectrometer was calibrated using an α-Fe foil at room temperature. The experimental spectra are presented relative to the centre of the α-Fe calibration spectrum.

3. Results and Discussion

$YCo_{12}B_6(^{57}Fe)$

Fig. 1 shows the ^{57}Fe Mössbauer spectra of $YCo_{12}B_6(^{57}Fe)$ at room temperature (Figs 1*a,b*) and $4\cdot2$ K (Fig. 1*c*). The dominant feature of the room-temperature spectrum is the central paramagnetic doublet characteristic of the 1-12-6 phase (Rosenberg *et al.* 1992; Campbell *et al.* 1993). The room-temperature spectrum on the extended velocity scale (Fig. 1*a*) allows us—assuming the same value of recoil-free fraction for all phases—to determine the extent of the impurity phases containing ^{57}Fe to be ~23% of the relative area of the Mössbauer spectrum. The
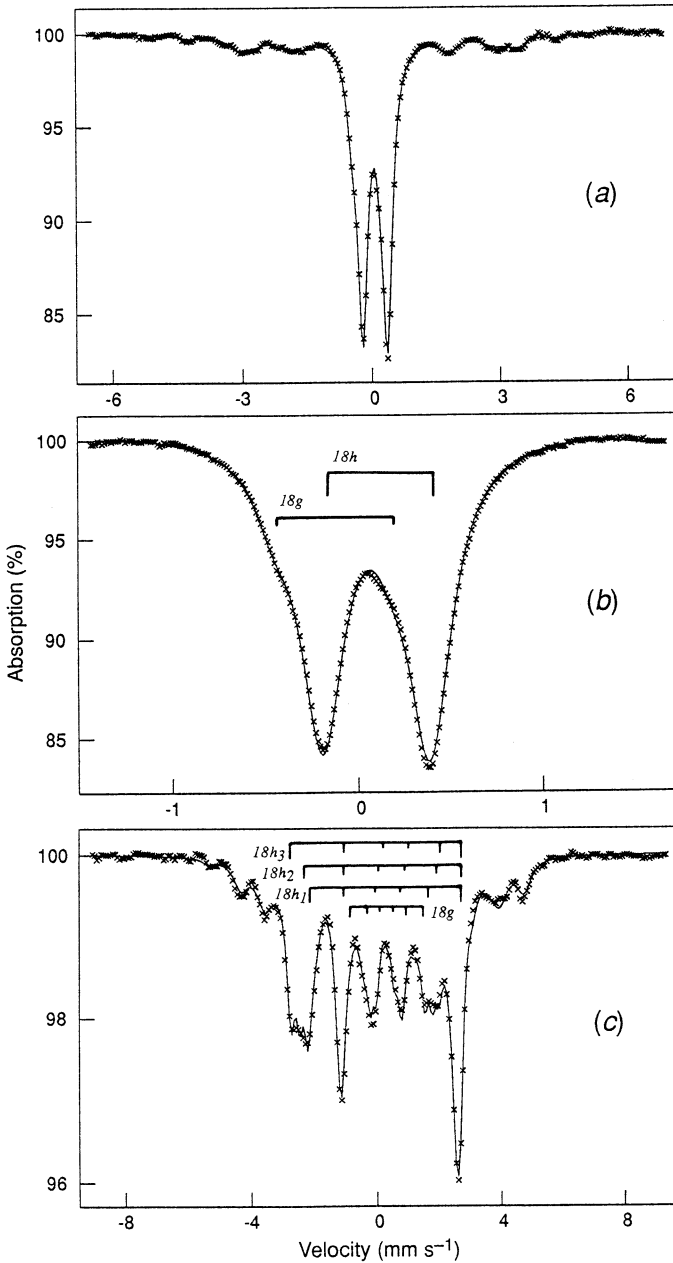
Fig. 1. ^{57}Fe Mössbauer spectra of $YCo_{12}B_6(^{57}Fe)$ at (a) room temperature (extended velocity scale), (b) room temperature (low velocity scale), and (c) 4·2 K. The fits to the spectra are described in the text. The stick diagrams in (b) show the locations and relative intensities of the doublets linked with the $18g$ and $18h$ sites. Similarly, the stick diagrams labelled $18g$, $18h_1$, $18h_2$, $18h_3$ in the 4·2 K spectrum (c) show the location and relative intensities of the four sextets used to fit the 1-12-6 spectrum.

mean values for the hyperfine magnetic field of the impurity phase ($20 \cdot 3$ T at room temperature and $25 \cdot 0$ T at $4 \cdot 2$ K) are consistent with the observation of the $Co_2B(^{57}Fe)$ phase in the XRD pattern (Murphy and Hershkowitz 1973).

Excluding the contribution of the $Co_2B(^{57}Fe)$ impurity phase to the experimental spectrum, the room-temperature spectrum of $YCo_{12}B_6(^{57}Fe)$ over the low velocity range (Fig. 1*b*) is well fitted by two overlapping paramagnetic doublets corresponding to ^{57}Fe occupying the 18*g* and 18*h* crystallographic sites in the 1-12-6 structure. The locations and relative intensities of these two doublets are indicated by the stick diagrams in Fig. 1*b* with the relative areas, quadrupole splittings (QS) and isomer shifts (IS) of these 1-12-6 subspectra given in Table 1. The relative areas of the two doublets (~89% and ~11%) have been obtained after accounting for the impurity phase, and thus refer solely to the 1-12-6 phase. As noted above, previous work on $RFe_{12-x}Co_xB_6$ compounds (R = La, Y, Cd) (Rosenberg *et al.* 1992) and $NdCo_{12}B_6$ (Campbell *et al.* 1993) showed that ^{57}Fe exhibits a strong preference for occupying the 18*h* sites, and the present observed relative areas for $YCo_{12}B_6$ are in good accord with this result.

Table 1. Hyperfine interaction parameters for $YCo_{12}B_6(^{57}Fe)$ and $NdCo_{12}B_6(^{57}Fe)$ at room temperature (cf. Figs 1*b* and 2*b* respectively)

Errors: QS $\pm 0 \cdot 02$ mm s^{-1}; IS $\pm 0 \cdot 01$ mm s^{-1}; FWHM $\pm 0 \cdot 01$ mm s^{-1}; relative area $\pm 5\%$

Sample	Component	QS (mm s^{-1})	IS (mm s^{-1})	FWHM (mm s^{-1})	Relative area (%)
$YCo_{12}B_6$	18*g*	$0 \cdot 63$	$-0 \cdot 13$	$0 \cdot 23$	11
	18*h*	$0 \cdot 58$	$0 \cdot 10$	$0 \cdot 24$	89
$NdCo_{12}B_6$	18*g*	$0 \cdot 87$	$0 \cdot 02$	$0 \cdot 27$	16
	18*h*	$0 \cdot 64$	$0 \cdot 10$	$0 \cdot 27$	84

Table 2. Hyperfine interaction parameters for $YCo_{12}B_6(^{57}Fe)$ at $4 \cdot 2$ K (cf. Fig. 1*c*)

Errors: B_{hf} $\pm 0 \cdot 5$ T; QS $\pm 0 \cdot 02$ mm s^{-1}; IS $\pm 0 \cdot 01$ mm s^{-1}; relative area $\pm 5\%$

Component	B_{hf} (T)	QS (mm s^{-1})	IS (mm s^{-1})	Relative area (%)
$18h_1$	$14 \cdot 9$	$0 \cdot 04$	$0 \cdot 20$	28
$18h_2$	$15 \cdot 5$	$-0 \cdot 31$	$0 \cdot 20$	22
$18h_3$	$16 \cdot 9$	$-0 \cdot 45$	$0 \cdot 21$	32
$18g$	$7 \cdot 0$	$0 \cdot 04$	$0 \cdot 20$	18

Fig. 1*c* shows the $4 \cdot 2$ K spectrum for $YCo_{12}B_6(^{57}Fe)$; at which temperature the 1-12-6 phase is ferromagnetic. Using the Mössbauer thermal scan technique we have measured the Curie temperature of $YCo_{12}B_6(^{57}Fe)$ and found it to be $T_C \simeq 167 \pm 5$ K, in general agreement with the magnetisation measurements of Mittag *et al.* (1989). After subtracting the spectral contribution of the $Co_2B(^{57}Fe)$ impurity phase to the overall spectrum of Fig. 1*c* we find that the magnetic 1-12-6 spectrum cannot be fitted with two sextets in the relative subspectral ratio found for the two doublets in the room-temperature paramagnetic spectrum (Fig. 1*b*). Attempts to fit the $4 \cdot 2$ K spectrum with two subspectra led to unrealistically large values for the linewidths (FWHM) and even then the fit was poor. Rather, the $4 \cdot 2$ K spectrum of the $YCo_{12}B_6$ compound is well fitted with four sextets,

three of which have roughly equal areas and magnetic hyperfine fields (B_{hf}) differing by only about 1 T. This analysis led to physically realistic linewidth values, similar to those obtained for the analysis of the room-temperature spectra of the $YCo_{12}B_6$ and $NdCo_{12}B_6$ compounds (Table 1). The fourth sextet has a smaller relative area and a much smaller hyperfine field than those of the three 'primary' sextets. The relative areas and hyperfine parameters of the four 1-12-6 sextets are given in Table 2. The ratio of the combined areas of the three primary sextets to that of the fourth smaller sextet is ~82% : 18% and we can therefore assign the three primary sextets (labelled $18h_1$, $18h_2$, $18h_3$ in Table 2) to the $18h$ site, and the fourth sextet, having a much smaller hyperfine field, to the $18g$ site. The locations and relative areas of these four sextets are indicated by the stick diagrams in Fig. 1c. This site assignment is consistent with previous work on 1-12-6 compounds (Rosenberg *et al.* 1992; Campbell *et al.* 1993). In Campbell *et al.* (1993), we outlined the argument that allows us to assign the sextet having the larger hyperfine field to ^{57}Fe occupying the crystallographic $18h$ site. Briefly, the $18h$ site has two more transition metal nearest neighbours than the $18g$ site, and one less rare-earth nearest neighbour, leading to a larger hyperfine field at the $18h$ site.

The observation of four sextets in the 4·2 K spectrum of the 1-12-6 phase rather than two indicates that the easy direction of magnetic ordering of the Co sublattice is not along the crystallographic c-axis and, as discussed below, is most likely to lie in the basal plane. The splitting of the $18h$ spectrum has been ascribed to the effects of anisotropic orbital moment contributions when the magnetisation direction is other than parallel to the c-axis (Erdmann *et al.* 1988). It is well known from numerous studies (e.g. Mitchell *et al.* 1989) that the transition metal (TM) sublattice anisotropy energy in R–TM–B ternary intermetallic phases is usually well described by a single term of the form $K_1 \sin^2 \theta$, where θ is the angle between the TM magnetisation and the c-axis. In the absence of other anisotropic effects this leads to magnetisation directions either parallel ($\theta = 0°$) or perpendicular ($\theta = 90°$) to the c-axis. Our Mössbauer results therefore suggest planar ordering of the Co sublattice in the 1-12-6 phase at 4·2 K.

$NdCo_{12}B_6(^{57}Fe)$

Fig. 2 shows room-temperature Mössbauer spectra of $NdCo_{12}B_6(^{57}Fe)$ recorded over extended (Fig. 2a) and low (Fig. 2b) velocity scales. Two magnetic sextets with hyperfine fields of 31·3 T (~18% area) and 24·5 T (~8% area) are observed in these spectra and are due to α-Fe-type and $Co_2B(^{57}Fe)$-type impurity phases. The analyses of these spectra have been presented in our previous paper (Campbell *et al.* 1993). Briefly, after accounting for the impurity components, the room-temperature $NdCo_{12}B_6(^{57}Fe)$ spectrum comprises two paramagnetic doublets with relative areas ~82% and ~18%, showing the strong $18h$ site preference of the ^{57}Fe atoms, similar to the case of $YCo_{12}B_6(^{57}Fe)$ described above. The location and relative intensities of these doublets are shown by the stick diagrams in Fig. 2b, with the hyperfine parameters of the $NdCo_{12}B_6(^{57}Fe)$ spectrum at room temperature given in Table 1.

In Fig. 3 we show the Mössbauer spectra of $NdCo_{12}B_6(^{57}Fe)$ recorded at various temperatures between 4·2 K and 175 K. As discussed previously (Campbell *et al.* 1993) the 4·2 K spectrum of $NdCo_{12}B_6(^{57}Fe)$ is well fitted with two magnetic

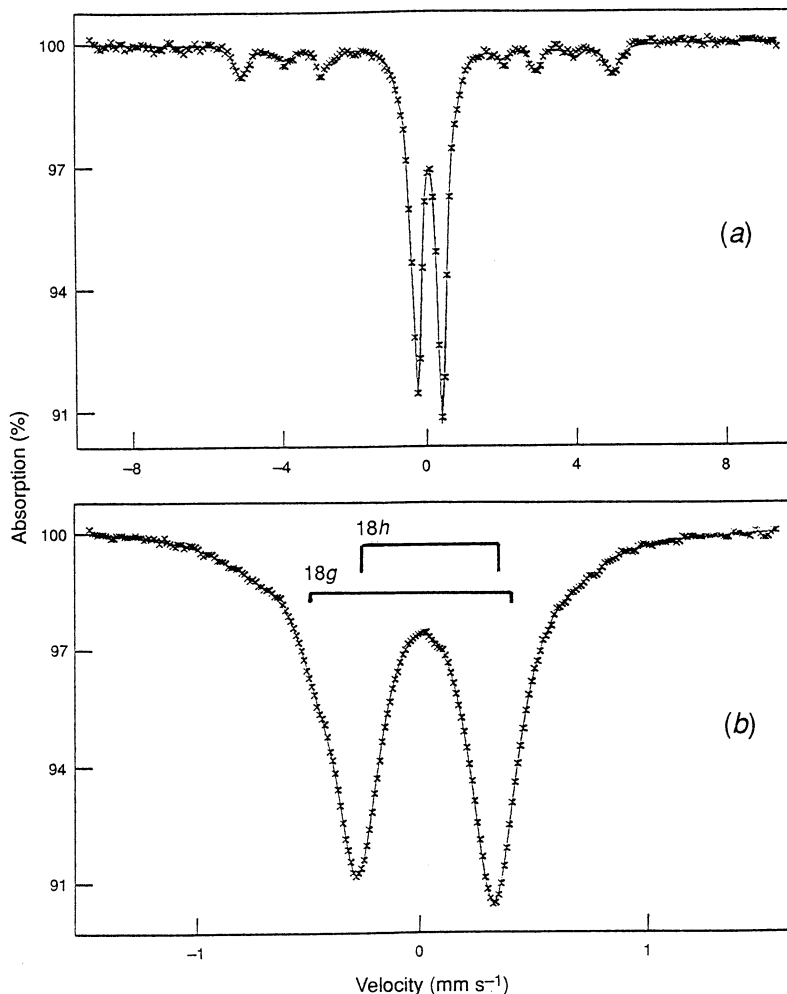**Fig. 2.** Room temperature Mössbauer spectra of $NdCo_{12}B_6(^{57}Fe)$: (*a*) extended velocity scale, and (*b*) low velocity scale. [See text for details of the fits; the stick diagrams in (*b*) show the locations and relative intensities of the $18g$ and $18h$ doublets.]

sextets with relative areas $\sim 81\%$ and $\sim 19\%$ and hyperfine fields of $15 \cdot 3$ T and $7 \cdot 0$ T, respectively. The sextet with the larger field is due to ^{57}Fe in the $18h$ sites.

From inspection of Fig. 3, it is immediately apparent that, unlike the $4 \cdot 2$ K spectrum, the 1-12-6 component of the magnetic spectra with $T \gtrsim 55$ K cannot be fitted with two simple sextets. We have analysed these spectra in a manner similar to the analysis of the $4 \cdot 2$ K spectrum of $YCo_{12}B_6(^{57}Fe)$, i.e. in terms of three primary sextets with similar areas and hyperfine fields, corresponding to the $18h$ site, and a fourth sextet with smaller area and field, corresponding to the $18g$ site. Fig. 4 shows the variation of the magnetic hyperfine fields for $NdCo_{12}B_6(^{57}Fe)$ for the three $18h$ sites, labelled $18h_1$, $18h_2$ and $18h_3$, and the $18g$ site as a function of temperature. The ferromagnetic ordering temperature was determined by the thermal scan technique and found to be $T_C = 168 \pm 3$ K,
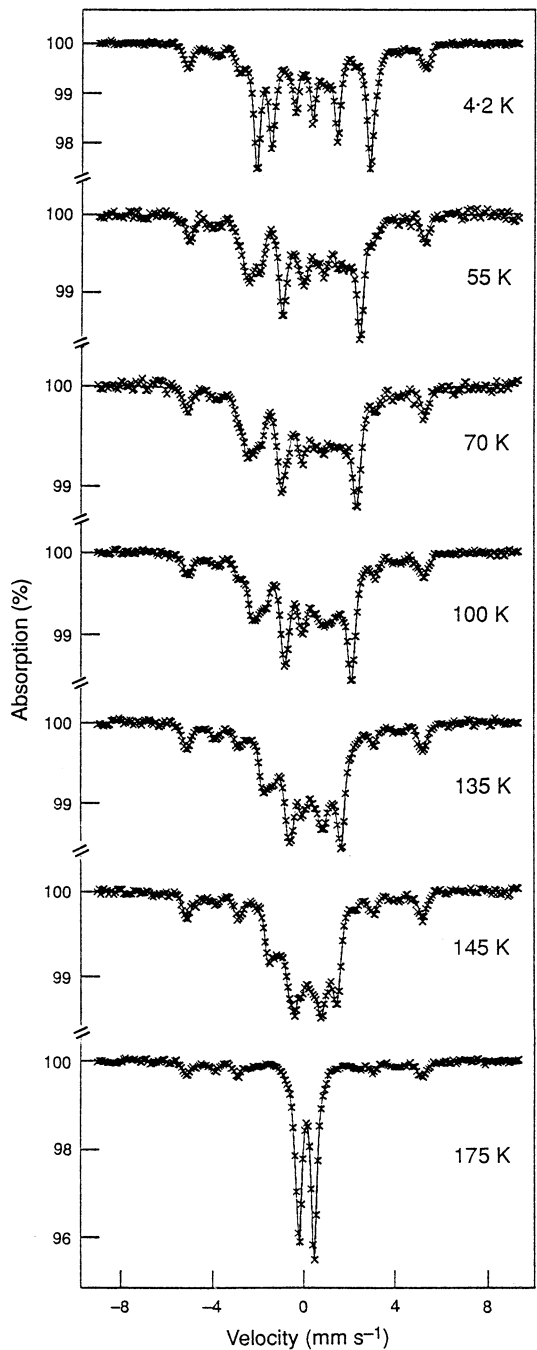
Fig. 3. ^{57}Fe Mössbauer spectra of NdCo$_{12}$B$_6$(^{57}Fe) at 4·2 K, 55 K, 70 K, 100 K, 135 K, 145 K and 175 K (see text for details of the fits).
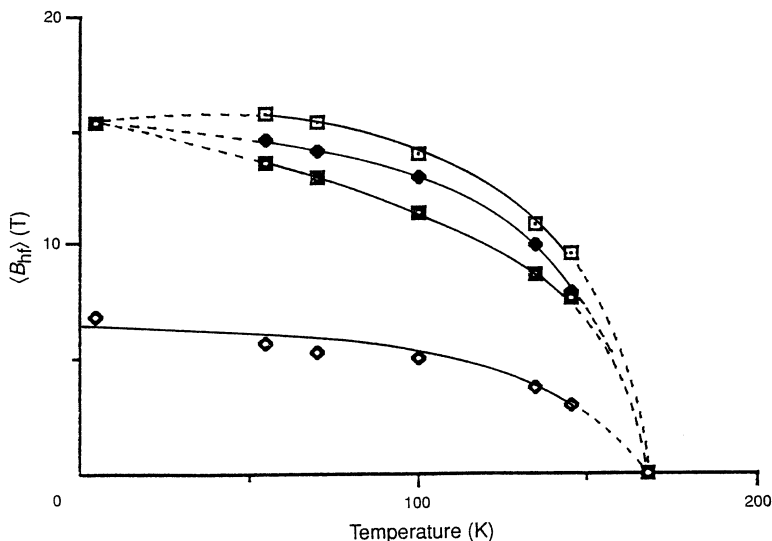
Fig. 4.   Magnetic hyperfine field values for the 18g ($\diamond$) and 18h sites of NdCo$_{12}$B$_6$(^{57}Fe) versus temperature. One subspectrum is used to describe the 18h site at 4·2 K, with three subspectra being required to describe the 18h site for the $T \gtrsim 55$ K data ($\blacksquare$ 18h_1; $\blacklozenge$ 18h_2; $\square$ 18h_3; see text for details of the fits). The curves are shown as guides to the eye.

agreeing well with the observed variation in B_{hf} for the various sites (Fig. 4). It should be noted that the use of one sextet to represent the mean magnetic hyperfine field of the 18h site at 4·2 K, compared with the three sextets required at higher temperatures, leads to an apparent increase in the magnetic hyperfine field for the 18h_3 site at $T \sim 55$ K (Fig. 4).

Clearly, the magnetic ordering direction of NdCo$_{12}$B$_6$(^{57}Fe) changes between 4·2 K and 55 K. The fact that the 4·2 K spectrum is well fitted with a single sextet due to each of the transition metal crystallographic sites indicates that the magnetic ordering direction is either parallel to the c-axis or close to it, since no magnetic splitting of the crystallographically equivalent sites is observed. Using the same argument as for YCo$_{12}$B$_6$(^{57}Fe), the magnetic spectra of NdCo$_{12}$B$_6$(^{57}Fe) for $T \gtrsim 55$ K are indicative of a magnetic ordering direction in, or close to, the crystallographic basal plane.

Our Mössbauer results therefore indicate that (i) the easy magnetisation direction of the Co sublattice is in the basal plane, and (ii) NdCo$_{12}$B$_6$ undergoes a spin-reorientation from c-axis to basal plane with increasing temperature, with a spin-reorientation temperature between 4·2 K and 55 K. It should be mentioned, however, that at this stage we cannot dismiss the possibility of canted magnetic structures.

Crystal Fields

The axial Nd anisotropy at 4·2 K dominates the planar Co anisotropy and is related to the Nd^{3+} crystal field interactions. Within the rhombohedral $R\bar{3}m$

structure, the Nd occupies the $3a$ crystallographic site with point symmetry $\bar{3}m$. Thus the Nd^{3+} crystal field Hamiltonian may be written (in standard notation) as

$$\mathcal{H} = B_{20}O_{20} + B_{40}O_{40} + B_{43}O_{43} + B_{60}O_{60} + B_{63}O_{63} + B_{66}O_{66} \,. \qquad (1)$$

We note here that rhombohedral structures are often indexed in terms of a hexagonal lattice. Nevertheless, the 'hexagonal' crystal field Hamiltonian, in which $B_{66}O_{66}$ is the only off-diagonal term, is inappropriate for rhombohedral structures.

The only crystal field information available on the $RCo_{12}B_6$ compounds at present is due to Gubbens et al. (1990) who fitted the temperature dependence of the ^{166}Er hyperfine magnetic field and quadrupole splitting deduced from ^{166}Er Mössbauer measurements on $ErCo_{12}B_6$. Using a simple exchange plus diagonal crystal field Hamiltonian, Gubbens and coworkers deduced the following crystal field parameters (relevant to Er^{3+}):

$$B_{20} = -0 \cdot 39 \text{ K}; \ \ B_{40} = -0 \cdot 5 \times 10^{-2} \text{ K and } B_{60} = -0 \cdot 2 \times 10^{-4} \text{ K}\,.$$

These parameters can be scaled to give the corresponding Nd^{3+} parameters if one assumes no change in the relevant crystal field lattice summations, such as A_{20} (standard notation). Using the appropriate Stevens (1952) constants and the 4f electronic radial averages (Freeman and Desclaux 1979), we deduce the following Nd^{3+} parameters:

$$B_{20} = +1 \cdot 54 \text{ K}; \ \ B_{40} = +7 \cdot 5 \times 10^{-2} \text{ K and } B_{60} = +1 \cdot 02 \times 10^{-4} \text{ K}\,.$$

However, these parameters predict a basal plane ordering of $NdCo_{12}B_6$ at $4 \cdot 2$ K and so are inconsistent with our experimental observations.

We have carried out point-charge model calculations for the R^{3+} ions in the $RCo_{12}B_6$ structure, and these predict that $A_{20} < 0$. Hence, B_{20} should be positive for Nd^{3+}, in agreement with the above deduction based on the $ErCo_{12}B_6$ work of Gubbens et al. (1990). In order to get axial ordering of $NdCo_{12}B_6$ at low temperatures, we therefore need B_{40} and/or B_{60} to be negative, opposite to the deduced values above. We note that the temperature dependence of the ^{166}Er hyperfine data reported by Gubbens et al. (1990) are low-temperature values up to $T/T_C \sim 0 \cdot 35$, and that the off-diagonal crystal field terms in equation (1) were ignored. Furthermore, the ^{166}Er spectra are complicated by electronic relaxation effects.

Clearly, more experimental data on the $RCo_{12}B_6$ compounds are required to enable us to determine a set of crystal field parameters appropriate to this phase. For example, we have shown that the Co sublattice exhibits easy-plane anisotropy, whereas Gubbens et al. (1990) claim c-axis ordering in $ErCo_{12}B_6$ at low temperature. Hence, as rare-earth anisotropy generally decreases faster than transition metal anisotropy with increasing temperature, it is likely that $ErCo_{12}B_6$ will exhibit a spin-reorientation. Data such as spin-reorientation temperatures provide invaluable information for the determination of crystal field parameters.

4. Conclusions

On the basis of ^{57}Fe Mössbauer-effect spectroscopy of $NdCo_{12}B_6$ and $YCo_{12}B_6$ doped with enriched ^{57}Fe, we have shown that the Co sublattice anisotropy in the $RCo_{12}B_6$ compounds is planar. At $4 \cdot 2$ K, $NdCo_{12}B_6$ orders along or close to the crystal c-axis, and undergoes an axis–plane spin-reorientation in the temperature range $4 \cdot 2$–55 K. At this stage the possibility of canted magnetic structures cannot be ruled out.

Acknowledgments

References

Buschow, K. H. J. (1987). *In* 'Proc. 9th Int. Workshop on Rare Earth Magnets, Bad Soden' (Eds C. Herget and R. Poersche), p. 453 (Deutsche Physikalische Gesellschaft: Bad Honef).
Campbell, S. J., Cadogan, J. M., Zhao, X. L., and Wu, E. (1993). *Hyperfine Interactions* (in press).
Chaban, N. F., and Kuz'ma, Yu. B. (1977). *Izv. Akad. Nauk SSSR Neorg. Mater.* **13**, 923.
Erdmann, K., Rosenberg, M., and Buschow, K. H. J. (1988). *J. Appl. Phys.* **63**, 4113.
Freeman, A. J., and Desclaux, J. P. (1979). *J. Magn. Magn. Mater.* **12**, 11.
Gubbens, P. C. M., van der Kraan, A. M., and Buschow, K. H. J. (1990). *J. Magn. Magn. Mater.* **87**, 276.
Jing, J., Campbell, S. J., and Pellegrino, J. (1992). *Meas. Sci. Technol.* **3**, 80.
Jurczyk, M., Pedziwiatr, A. T., and Wallace, W. E. (1987). *J. Magn. Magn. Mater.* **67**, L1.
Kuz'ma, Yu. B., Chernyak, G. V., and Chaban, N. F. (1981). *Dopov. Akad. Nauk. Ukr. RSR*, **12**, 81.
Mitchell, I. V., Coey, J. M. D., Givord, D., Harris, I. R., and Hanitsch, R. (Eds) (1989). 'Concerted European Action on Magnets (CEAM)' (Elsevier Applied Science: London).
Mittag, M., Rosenberg, M., and Buschow, K. H. J. (1989). *J. Magn. Magn. Mater.* **82**, 109.
Murphy, K. A., and Hershkowitz, N. (1973). *Phys. Rev.* B **7**, 23.
Niihara, K., and Yajima, S. (1972). *Chem. Lett.*, 875.
Rosenberg, M., Mittag, M., and Buschow, K. H. J. (1988). *J. Appl. Phys.* **63**, 3586.
Rosenberg, M., Sinnemann, T., Mittag, M., and Buschow, K. H. J. (1992). *J. Alloys Compounds* **182**, 145.
Stadelmaier, H. H., and Lee, H. J. (1978). *Z. Metall.* **69**, 685.
Stevens, K. W. H. (1952). *Proc. Phys. Soc.* A **65**, 209.

A Heuristic Account of the Electron–Phonon Coupling Mechanism in the Formation of Pre-martensite Tweed Structures*

Peter Norman

Department of Physics, Monash University,
P.O. Box 197, Caulfield East, Vic. 3145, Australia.

Abstract

Electron–phonon coupling has been proposed by a number of researchers as the probable mechanism involved in martensitic transformations of many metals and alloys. This paper provides a plausible account of the way in which Kohn anomalies may give rise to tweed microstructure in pre-martensitic phases of fcc and bcc crystals.

1. Introduction

The purpose of this paper is to demonstrate the way in which the periodic lattice displacements of tweed structure may be formed as the result of Kohn anomalies in both bcc and fcc crystals. Essentially, this demonstration is presented in diagrammatic form so that the relationships between the representations in direct and reciprocal space may be clearly seen. This work is an extension of the ideas of Krivoglaz (1969), Krivoglaz and Tu Hao (1968) and Moss (1969) who considered pre-martensitic anomalies in various alloys.

In the electron–phonon interaction mechanism outlined by Ashcroft and Mermin (1976) and Ziman (1969), the basic assumption is that the rate of sound attenuation associated with the lattice softening is related to the energy being lost by the phonons to the Fermi-surface electrons. This is so because when a sound wave propagates through a metal the microscopic electric fields due to the displacement of the ions can impart energy to electrons near the Fermi level, thereby removing energy from the wave. It should be noted that it is only those electrons near the Fermi surface that can affect the sound attenuation, since the exclusion principle forbids electrons with lower energies from exchanging small amounts of energy with the waves. Furthermore, it is the electrons near the external Fermi surface that play a dominant role since there are many more of them.

Axe and Shirane (1973) illustrated their discussion of displacive transformations in terms of the soft-mode concept with a simple one-dimensional representation of a longitudinal displacement wave in a periodic lattice with spacing a. They considered the case when the magnitude of the phonon wavevector q is equal to π/a so that the displacements of adjacent atoms are out of phase, as shown in Fig. 1. Such fluctuations with harmonic time dependence are Brillouin

---

zone-boundary phonons, and static displacements or displacive transformations can result if they become unstable. Axe and Shirane (1973) showed that, for the particular zone-boundary phonon pictured in Fig. 1, the associated displacive transformation involves a 'dimerisation' of the lattice particles and a doubling of the unit cell dimension, as shown in Fig. 2. This particular case has been thoroughly investigated by Peierls (1955) and the role of the Fermi surface has particular significance.
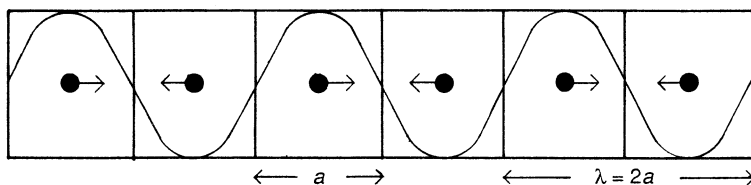

Fig. 1. Zone-boundary longitudinal phonon with wavevector $q = \pi/a$ in a periodic one-dimensional lattice.
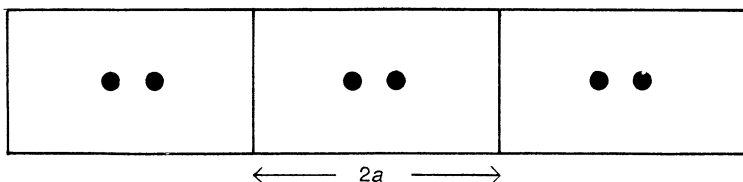

Fig. 2. 'Dimerisation' of lattice particles in a periodic one-dimensional lattice resulting from the displacive transformation produced by the softening of the zone-boundary phonon shown in Fig. 1.

In Sections 2 and 3 the basic principles of this illustration are used to explain the displacive transformations associated with a bcc alloy and a fcc alloy in terms of $\langle 110 \rangle$ and $\langle 111 \rangle$ transverse acoustic phonons respectively. Whereas Axe and Shirane (1973) accounted for the displacive transformation of 'dimerisation' in terms of the static displacement of single atoms in opposite directions, it is intended in the next sections to provide similar explanations of the formation of tweed microstuctures in terms of the static displacement of large groups of atoms in the same direction.

In discussing structural phase transformations, the range of correlations between the atomic displacements induced by a soft mode is designated as the correlation length ζ. Furthermore, the size of ζ is indicated in the corresponding diffraction patterns by the thickness $2\pi/\zeta$ of the relwalls of diffuse scattering. It has already been shown by Norman et al. (1985) and Finlayson et al. (1988) that the thickness of the diffraction relrods of $Cu_{51}Zn_{49}$ and $Fe_{68}Ni_{32}$ may be modelled by Kohn constructions. In the following sections it will be shown that the correlation lengths of the displaced atoms of each of these alloys are thereby related to the degree of overlap of the corresponding multiply-connected Fermi surfaces.

2. Electron–Phonon Coupling in the bcc Alloy $Cu_{51}Zn_{49}$

Fig. 3 is the reciprocal lattice diagram of $Cu_{51}Zn_{49}$ and includes the Fermi surface and related Brillouin zone boundaries depicted in the $(0\bar{1}0)$ plane. Also

shown is the solid arrow representing the $\langle 101 \rangle \langle 10\bar{1} \rangle$ transverse acoustic (TA) phonon satisfying the Kohn anomaly condition $q = 2k_F$, and the broken arrow representing the Fermi surface electron wavevector k_F in the $\langle 101 \rangle$ direction.
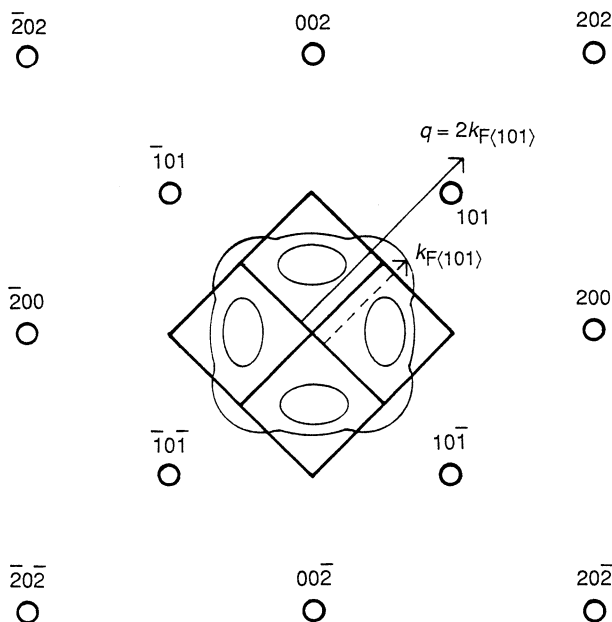

Fig. 3. Reciprocal lattice diagram of β-$Cu_{51}Zn_{49}$ in the $(0\bar{1}0)$ plane showing the Fermi surface and Brillouin zone boundaries. The Kohn anomaly wavevector $q = 2k_F$ is represented by the solid arrow.

Fig. 4 is the crystal lattice diagram of $Cu_{51}Zn_{49}$ showing the same two vectors as in Fig. 3. It can readily be seen that the phonon involves simultaneous displacements of atoms in $\langle 101 \rangle$ rows in $\langle 10\bar{1} \rangle$ directions. It is suggested that it is in this way that the large number of atoms constituting each of the basic units of a tweed pattern are displaced when pre-martensitic conditions prevail in this alloy. In this regard it is of particular interest to note that Figs 3 and 4 clearly indicate how the value of λ results in this phonon gradually getting out of phase with the periodicity of the crystal lattice in $\langle 101 \rangle$ directions. This is so because in Fig. 3 $q = 2k_{F,\langle 101 \rangle}$ is *slightly larger* than the spacing between 000 and 101 because $k_{F,\langle 101 \rangle}$ extends slightly beyond the Brillouin zone boundary. Accordingly, in Fig. 4 λ is *slightly less* than the interatomic spacing in the $\langle 101 \rangle$ direction.

It is therefore suggested that if the Fermi surface extends beyond the Brillouin zone boundary in the $\langle 101 \rangle$ direction by 1/50 of the distance from 000 to this boundary, then the pair of anti-phase domain boundaries corresponding to the opposite edges of a tweed cell would be 50 atoms apart.

Such pre-martensitic structural modulations may constitute nucleation sites for martensitic transformations. When β-brass is quenched, it rapidly orders to form the β^1 phase and simultaneously undergoes a martensitic transformation by forming plates of a close-packed structure which is basically fcc. The nucleation

and growth of a martensite plate is a complex process which takes place in several distinct stages. Of particular significance for this nucleation is $\langle 101 \rangle \langle 10\bar{1} \rangle$ shear. The stiffness of a bcc structure, such as β-brass, with respect to $\langle 101 \rangle \langle 10\bar{1} \rangle$ shear is given by the elastic modulus $c' = 0 \cdot 5(c_{11} - c_{12})$, and the ratio of c' to c_{44} is a measure of stability with respect to a close-packed structure. For
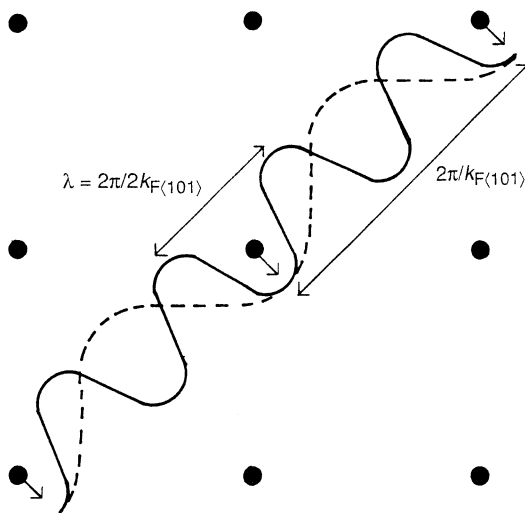

Fig. 4. Crystal lattice diagram of β-Cu$_{51}$Zn$_{49}$ in the $(0\bar{1}0)$ plane showing the Kohn anomaly phonon with wavelength λ.
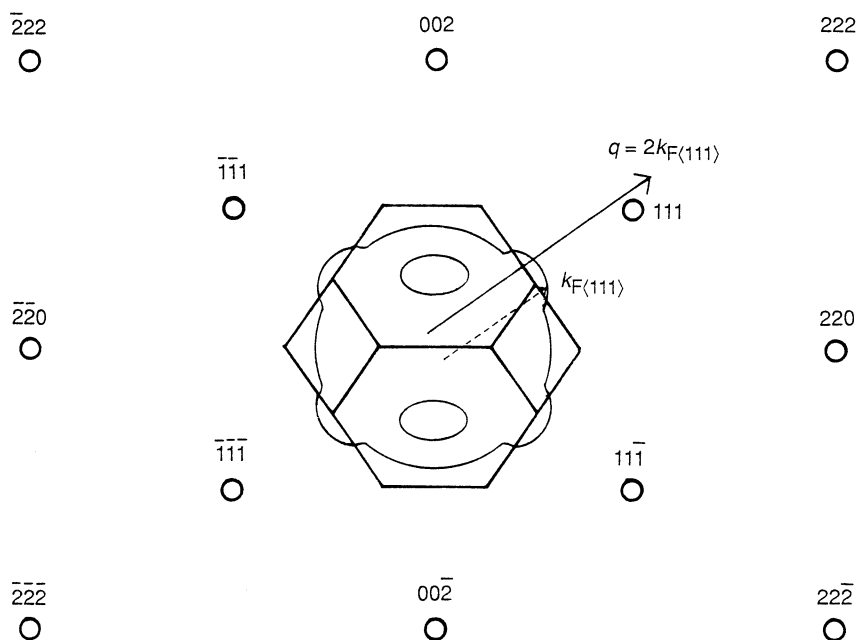

Fig. 5. Reciprocal lattice diagram of Fe$_{68}$Ni$_{32}$ in the $(1\bar{1}0)$ plane showing the Fermi surface and Brillouin zone boundaries. The Kohn anomaly wavevector $q = 2k_F$ is represented by the solid arrow.

β-brass, $c'/c_{44} = 1/18$ at room temperature. The absolute value of c' is low and it decreases as the temperature falls towards the transformation temperature, indicating that the resistance of the lattice to $\langle 101 \rangle \langle 10\bar{1} \rangle$ shear is small at the temperature of its transformation to a close-packed structure.

3. Electron–Phonon Coupling in the fcc Alloy Fe$_{68}$Ni$_{32}$

Fig. 5 is the reciprocal lattice diagram of Fe$_{68}$Ni$_{32}$ and includes the Fermi surface and related Brillouin zone boundaries depicted in the $(1\bar{1}0)$ plane. A significant $\langle 111 \rangle \langle 11\bar{2} \rangle$ TA phonon is also shown in a manner similar to the representation of $\langle 101 \rangle \langle 10\bar{1} \rangle$ phonons in Fig. 3.

Fig. 6 is the $(1\bar{1}0)$ crystal lattice diagram of Fe$_{68}$Ni$_{32}$. As in the case of Cu$_{51}$Zn$_{49}$ it can be seen how the boundaries of a tweed cell in Fe$_{68}$Ni$_{32}$ may arise as a $\langle 111 \rangle \langle 11\bar{2} \rangle$ TA phonon that satisfies the Kohn anomaly condition extends to atoms where the $\langle 11\bar{2} \rangle$ displacements are out of phase with those shown in Fig. 6.

Because $\langle 11\bar{2} \rangle$ displacements on $\{111\}$ planes in fcc structures are geometrically equivalent to $\langle 10\bar{1} \rangle$ displacements on $\{101\}$ planes in bcc structures, it is suggested that pre-martensitic nuclei in Fe–Ni alloys may be generated by the static atomic displacements produced by electron–phonon coupling in the same way as may occur in Cu–Zn alloys.
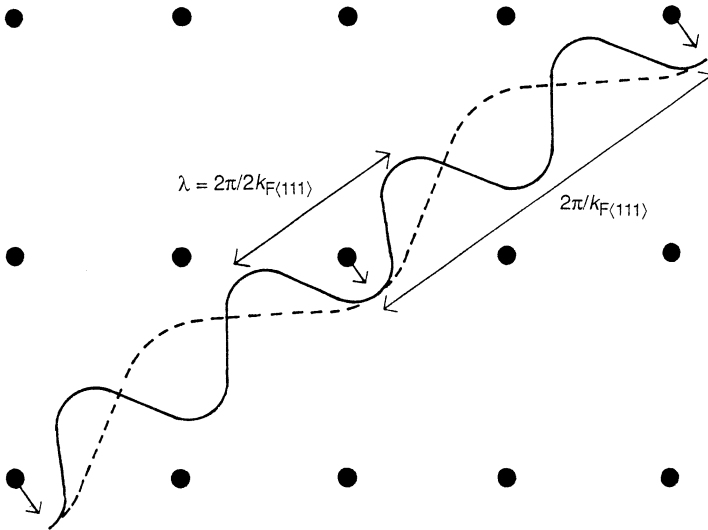

Fig. 6. Crystal lattice diagram of Fe$_{68}$Ni$_{32}$ in the $(1\bar{1}0)$ plane showing the Kohn anomaly phonon with wavelength λ.

4. Conclusion

The brief analysis outlined above appears to indicate the way in which electron–phonon coupling may give rise to the formation of tweed structure in both Cu$_{51}$Zn$_{49}$ and Fe$_{68}$Ni$_{32}$ alloys. It seems reasonable to suggest that the same mechanism may also be applicable to all those crystals that possess multiply-connected Fermi surfaces and exhibit tweed structure.

References

Ashcroft, N. W., and Mermin, N. D. (1976). 'Solid State Physics', pp. 275–7 (Holt, Rinehart and Winston: New York).
Axe, J. D., and Shirane, G. (1973). *Phys. Rev.* B **8**, 1965.
Finlayson, T. R., Morton, A. J., and Norman, P. D. (1988). *Metall. Trans.* A **19**, 199.
Krivoglaz, M. A. (1969). 'Theory of X-ray and Thermal Neutron Scattering by Real Crystals' (Plenum: New York).
Krivoglaz, M. A., and Tu Hao (1968). 'Defects and Properties of the Crystal Lattice' (Nankova Dumka: Kiev).
Moss, S. C. (1969). *Phys. Rev. Lett.* **22**, 1108.
Norman, P. D., Finlayson, T. R., and Morton, A. J. (1985). *Metals Forum* **8**, 250.
Peierls, R. E. (1955). 'Quantum Theory of Solids', pp. 108–11 (Oxford Univ. Press).
Ziman, J. M. (1969). 'Principles of the Theory of Solids', pp. 246–7 (Cambridge Univ. Press).